Mechanisms of Glass Corrosion by Aqueous Solutions

Roland Hellmann

Mechanisms of Glass Corrosion by Aqueous Solutions

Chapter 5.12

Encyclopedia of Glass Science, Technology, History, and Culture, Volume II, First Edition. Pascal Richet. Published 2021 by John Wiley & Sons, Inc.

https://doi.org/10.1002/9781118801017.ch5.12

Roland Hellmann, ISTerre, CNRS, Université Grenoble Alpes, CS 40700, 38058 Grenoble Cedex 9, France

Reviewers
J.P. Icenhower, Sandia National Laboratories, Carlsbad Program Group, Carlsbad, NM 88220, USA.

T. Geisler, Steinmann-Institut für Geologie, Universität Bonn, D-53115 Bonn, Germany

Abstract

Abiotic mechanisms of chemical alteration of glass are discussed in terms of the two principal theories currently existing. The first is the traditional leached-layer model, which is based on solid-state volume interdiffusion of preferentially leached cations from the glass with hydronium species (H_3O^+) from the bulk solution. This results in the formation of a so-called cation-leached layer that is characterized by broad, diffusion-like chemical depth profiles extending from the surface to the underlying pristine glass. The second theory is relatively new and postulates that glass corrosion is controlled by coupled interfacial dissolution-reprecipitation (CIDR). This mechanism is based on coupled interfacial chemical reactions that take place within a thin fluid film at the glass interface, resulting in a reprecipitated surface layer having a very sharp interface with the pristine glass substrate. Studies from the literature are discussed and critically analyzed to illustrate the application of these two competing theories to borosilicate glass alteration in the laboratory. Finally, the main parameters influencing glass corrosion kinetics are discussed, including those that lead to decreasing rates as a function of reaction progress.

1. Introduction

Chemical alteration by aqueous solutions is one of the most important processes undergone by glasses, either in industrial and environmental applications (Ch. 5.11), or naturally at the Earth's surface (Ch. 7.3). Induced by the intrinsic chemical instability of glass, aqueous alteration is referred to as corrosion in a laboratory setting, or chemical weathering in nature. Chemical weathering is due to the action of abiotic or biotic agents, or both, and plays a major role in controlling seawater chemistry and aqueous CO_2 uptake during dissolution [1], for example. Industrial and environmental applications of glass corrosion include the development of durable corrosion-resistant packaging (Ch. 7.7), in situ remediation of polluted water, carbon (CO_2) capture and storage, or secure, long-term isolation of industrial and nuclear waste (Ch. 9.9-10), [2]). Archaeometry is another important field associated with glass weathering, and can be used for dating of archeological glass objects and paleoclimate reconstructions [3].

Knowledge of the molecular-scale mechanisms of alteration is a prerequisite for understanding how glasses react with aqueous solutions, thereby permitting more accurate modeling of corrosion and long-term durability. Corrosion is characterized by a combination of physical and chemical processes leading to the formation of one or more surface altered layers at the expense of the pristine glass. These layers are primarily composed of elements derived from the dissolution of the glass, but typically also incorporate chemical species from the surrounding bulk solution. Separating the fresh glass from the solution, this near-surface zone has a varied terminology in the literature: leached layer, gel, surface altered layer, interfacial reprecipitate, palagonite. Because the phases making up this zone are intimately associated with the chemical alteration of the glass, understanding the details of their formation is crucial to elucidating corrosion mechanisms.

Two approaches are necessary to achieve this goal. The first aims at determining the chemical composition, structure and physical properties (*e.g.*, porosity, pore size distribution, permeability) of the surface altered layer(s); the second at studying the interfacial region that delimits the boundary between the pristine glass and the adjacent surface-altered layer. Critical to the development of a mechanistic model are accurate measurements of the chemical and structural gradients between these two phases. For this purpose, advanced analytical techniques having very high spatial resolution, elevated mass resolution, or both, should be used.

In this chapter, the discussion of corrosion mechanisms is largely based on a historical-chronological presentation. Two early models that characterized the state of knowledge up to the mid-1980s are first described [4], followed by the traditional model based on preferential cation leaching and interdiffusion. Frequently called the leached-layer model, it combines many of the elements found in the two early models. It has held sway over the past three decades and is still the predominant mechanism in the literature. The last model treated is relatively new and is based on coupled interfacial dissolution-reprecipitation (CIDR). Acceptance of this mechanism, initially developed in mineralogy and geochemistry, has been quite contentious, but has nevertheless been gaining attention in the glass community.

List of acronyms (cf. Ch. 2.3 and 5.1)

APT: Atom Probe Tomography

EDX: Energy-Dispersive X-ray spectroscopy

CIDR: Coupled Interfacial Dissolution-Reprecipitation

EFTEM: Energy Filtered TEM

EPMA: Electron-Probe MicroAnalysis

FIB: Focused Ion-Beam milling

HAADF: High-Angle Annular Dark Field

HRTEM: High-Resolution TEM

RBS: Rutherford Backscattering Spectrometry

RNRA: Resonant Nuclear Reaction Analysis

SIMS: Secondary-Ion Mass Spectrometry, including nano- and Time-of-Flight-SIMS

STEM: Scanning TEM

XPS: X-ray Photoelectron Spectroscopy

2. Early models

Dran and colleagues [4] summarized the two prevailing models regarding the aqueous dissolution of silicate glasses that held sway in the mid-1980's. The first was thought to apply to chemically complex or natural glasses. Its proponents postulated an overall congruent dissolution process,

characterized by the stoichiometric release of both framework and network-modifying elements. As dissolution proceeds, the concentrations of silica and other elements build up in the bulk solution, so that upon reaching saturation, one or more secondary crystalline phases (generally silicates) precipitate onto the glass surface (Fig. 1a). The alternate model was relevant to chemically simple, laboratory-produced glasses. It is based on the in situ preferential release of mobile, network modifying cations (*e.g.*, Na^+, Li^+, K^+) into the bulk solution. Keeping the relict, leached glass structure electrically neutral requires replacement of the leached cations by H ions (most likely H_3O^+) from the bulk solution; this process may also be accompanied by the influx of molecular H_2O into the leached layer. The outer edge of the silica-rich leached layer releases Si and O to the bulk solution through chemical hydrolysis reactions (Fig. 1b). Interestingly, one or the other mechanism has been used to account for the alteration of volcanic glasses depending on their age [5].

3. Leached-layer model

3.1. The standard model

The current generalized approach to glass corrosion has many similarities with the two early models. The altered zone, or leached layer, is comprised of three separate entities (Fig. 2). Adjacent to the pristine glass is an interdiffusion zone or layer, which is characterized by preferential removal of cations and sigmoidal chemical profiles, and is sometimes referred to as a hydrated glass layer [6]. Following this layer is a gel layer composed primarily of hydrated silica, where all the elemental concentrations are relatively constant. In the first stages of corrosion, the glass structure at the surface is progressively transformed by the selective leaching of certain cations (alkali and alkaline earth network modifiers, as well as network-formers such as B) [2,7-14]. For the interdiffusion zone to remain electro-neutral, the preferentially released cations are replaced by H ions (*i.e.*, H_3O^+) from the bulk solution. Each H_3O^+-cation couple (*e.g.*, H_3O^+- Na^+, H_3O^+- Ca^{2+}, H_3O^+- B^{4+}) can be characterized by a single interdiffusion coefficient that depends on the individual diffusion coefficients of both components. In other words, the outward diffusion rates of cations are coupled to the rate-determining (slower) inward diffusion rates of H ions. For simplicity, only two profiles representing a single interdiffusion couple are shown in Fig. 2, whereas in reality there will

be multiple interdiffusion profiles with different gradients and depths, depending on the charge of the cation (*i.e.*, interdiffusion of H_3O^+- B^{4+} will be significantly slower, and thus shallower, than H_3O^+- Na^+).

Throughout the process, the inner interface of the diffusive layer (the diffusion front in Fig. 2) continuously advances into the glass at a rate characteristic of solid-state volume interdiffusion. This process is the same as in the early model (Fig. 1b), in particular because the leached, relict zone remains covalently bonded to the pristine glass via Si-O linkages [7]. The outer interface of the diffusion layer is where silica is released to solution. Because of its relict nature and the sigmoidal shape of its diffusion profiles, the leached layer should not have a sharp structural and chemical interface with the pristine glass. At a significantly higher reaction progress (ξ), a separate porous gel layer composed primarily of hydrated silica begins to form on top of the diffusive layer, mainly by hydrolysis and condensation reactions. Hence, the diffusive zone advances by interdiffusion into the pristine glass at its inner interface, and is consumed by gel formation at its external interface [2,7-9,14,15].

Once the gel layer has formed and continues to grow, silica is released both at the outer interface of the interdiffusion layer, as well as at the external boundary of the gel in contact with the bulk solution. However, silica resorption can occur throughout the gel layer when aqueous silica becomes saturated in the bulk solution and within the gel pores [2]. These processes are sketched in Fig. 2 as (i) inward H ion diffusion; (ii) counterbalanced outward diffusion of preferentially released cations; (iii) silica release (straight dark arrows); and (iv) silica resorption (curved dark arrows). A net balance of all these rates governs the overall thicknesses of the interdiffusion and gel layers over time. The pronounced porosity of the gel layer allows for the unimpeded inward and outward flux of reactants and products between the bulk solution and the diffusive zone-pristine glass interface. In some cases, however, eventual pore closure in the gel layer may retard the overall corrosion process [16]. Moreover, depending on the composition of the glass, alteration conditions, and composition of the bulk solution, aggregates of secondary crystalline phases (zeolites, phyllosilicates, metal oxyhydroxides, hydrosilicates) may precipitate (Fig. 2) on top of the gel as a third layer [2,7-9,15,17].

The attributes of this model are well illustrated in a study [9] of the 3-month aqueous alteration of SON68 borosilicate at pH 8 and 90 °C (Fig. 3), a chemically complex analog of the glass produced at La Hague, France for storing nuclear waste [7]. The three different layers illustrated in Fig. 2 are apparent in the chemical depth profiles (Fig. 3) determined by SIMS. The leached layer consists of an inner interdiffusion zone (where sigmoidal B and Li profiles are anti-correlated with a roughly sigmoidal H profile) and an outer gel (where depleted B and Li, and enriched H concentrations are relatively constant), on top of which phyllosilicates have crystallized as a porous layer. Currently the leached layer model of glass corrosion, as exemplified by Fig. 3, is the most widely accepted, in particular within the established glass community. It is the basis for nearly all codes modeling the macroscale chemical alteration of glasses in aqueous solutions (*e.g.*, GRAAL [7]).

3.2. A complex hybrid model

A major concern with most studies supporting the leached layer mechanism is that the depths and gradients of the measured chemical profiles strongly depend on the analytical techniques used. This is illustrated by the results of a 25.75-year laboratory experiment [6], whose authors were among the first to study glass corrosion with atom probe tomography (APT), a very powerful technique that can provide 3-dimensional reconstructions of the chemical and isotopic composition of a sample with sub-nanometer depth and lateral spatial resolution, as well as very high mass resolution ($m/\Delta m$ = 1000, FWHM).

In this study, SON68 glass was altered at 90 °C and pH 7.0-7.2 in a slowly renewed granitic groundwater solution. From SEM observations, the sample consisted of the pristine glass, a hydrated (diffusive) glass layer (1000 nm), a gel layer (7500 nm) and surficial crystalline phases (a few 100s of nm), yielding a total alteration thickness of approximately 9000 nm. High-resolution chemical profiles at the pristine glass-hydrated glass interface, determined by APT (Fig. 4), reveal smooth decreases of Li, Na, B and Al concentrations with increasing depth from the pristine glass interface, with gradient widths of ≈ 50 nm, and up to ≈100 nm for Na (Fig. 4a). On the other hand, Si and H show smooth enrichment trends from the pristine glass interface, with gradient widths of 40-50 nm, whereas K (originating mainly from the granitic solution) and Ca increase over distances of 10-20 nm and 100 nm. Much sharper gradient widths for Na and B (3-4 nm), K (5 nm), Li (17

nm), and H (20 nm) were also observed in this study (Fig. 4b). Taken together, these results were interpreted in terms of a two-stage mechanism. First, an initial preferential loss of Li by interdiffusion with H occurred, which led to sigmoidal, anti-correlated Li and H profiles that became relatively constant after 15-20 nm. Subsequently, Na and B were preferentially released by dissolution, creating very sharp dissolution front profiles (Fig. 4b), with strong depletion at depths > 15 nm.

In this hybrid model, an interdiffusion process has been combined with preferential dissolution, resulting in a steep interdiffusion front that is partially coincident in space with an even sharper dissolution front within the hydrated glass layer (Fig. 5). The entire hydrated layer is by their definition a product of interdiffusion [6], but the results indicate that the diffusion profiles only extend to a depth of 20 nm from the interface with the pristine glass (Fig. 4b). Diffusion modeling of leached layers [18,19] shows that a 1000-nm thick diffusion zone characterized by a thin and steep diffusion front occupying only 20 nm at the inner extremity is physically not reasonable. In other words, the leached-layer model cannot explain how the remaining 980 nm of the hydrated layer forms, and in particular, why over the course of 25.75 years the Li and H profiles remained so sharp and so close to the interface with the pristine glass, although at the same time silica dissolution should have been occurring at the expense of the outer interface of the hydrated glass layer. Moreover, the K profile is anti-correlated with those of Na and B, and mimics them in terms of sharpness and position with respect to the dissolution front. However, K had presumably diffused into the diffusive zone from the solution, a scenario that should have led to a K profile mimicking those of H and Li.

The suggestion of a hybrid diffusion-dissolution process occurring near the pristine glass interface is interesting, but whether this is physically realistic can be questioned. In particular, this process assumes that solid-state volume interdiffusion in a glass at 90 °C is faster than competing chemical hydrolysis reactions (*e.g.*, [20]). If true, one could ask why the diffusion and dissolution fronts would still be nearly spatially commensurate after nearly 26 years in spite of their significantly different rates. The Li ion is small and carries a +1 charge, whereas the inward diffusing, charge-compensating H species (most likely H_3O^+) is significantly larger so that it will be much slower than Li and, thus, be rate determining in the Li-H diffusion couple [18,19]. The ultimate question is,

therefore, whether the Li and H profiles represent true interdiffusion, or an entirely different process? An alternative and physically more realistic explanation of the sharp chemical gradients measured, in particular for Li, Na, B, and K, is the coupled interfacial dissolution-reprecipitation mechanism.

4. Coupled interfacial dissolution-reprecipitation (CIDR)

4.1. High-resolution analyses

Regardless of the particular manner in which chemical profiles are theoretically interpreted, a fundamental point is that the need for high-resolution data is primordial. Two types of recent experimental and analytical advances fulfill this necessity. The first involves sample-preparation techniques, initially ultramicrotomy [5,15,21,22] and more recently, focused ion-beam (FIB) milling [23]. Not only have these techniques allowed altered mineral and glass specimens to be prepared in cross section, but also thin enough to be electron transparent and therefore analyzable by TEM techniques. These advances have eliminated the need to use SIMS, XPS, RNRA, RBS or EPMA to measure chemical depth profiles. These techniques are based on successive measurements starting from the top of the surface altered layer, proceeding downwards through the layer, and finally finishing in the pristine mineral or glass. More importantly, their beam footprints range from tens of μm to several mm; when applied to samples with rough surfaces and irregular internal interfaces, the ensuing chemical profiles are artificially enlarged (*i.e.*, smeared out), making them considerably wider than they really are.

The second important advance has been the use of analytical techniques having extremely high spatial resolution (Table 1), with beam footprints in the nanometer to sub-nanometer range, to measure surface-altered layers directly in ultrathin electron-transparent cross sections. These techniques, primarily TEM combined with electron-energy filtering (EFTEM) and electron energy-loss spectroscopy (EELS), or STEM-EDX (scanning TEM-energy dispersive X-ray spectroscopy), have yielded novel nanometer-scale resolved chemical maps of the interfacial region encompassing the unaltered primary phase and the secondary surface altered layer(s). Moreover, high-resolution chemistry measurements of glass corrosion by TEM have recently been complemented by the

application of APT, whereas isotope-tracer experiments have provided unique insights into the dynamic nature of the corrosion process.

The power of these new approaches has been demonstrated by the nm-sharp chemical and structural interfaces evidenced in altered minerals (*e.g.*, [19,22,24]) and glasses (*e.g.*, [6,16,21,25-27]). Spatially commensurate chemical and structural interfaces, which are very sharp at the nanometer to subnanometer-scale, bear none of the hallmarks of diffusion, namely smooth and broad sigmoidal chemical profiles spanning the region between the pristine glass interface and the outer boundary of the gel [18-20]. Likewise, the formation of rhythmic and patterned alteration layers with sharp chemical and isotopic boundaries reflect chemical self-organization processes that are difficult to reconcile with a preferential cation leaching-interdiffusion mechanism. In summary, techniques such as APT, EFTEM and STEM-HAADF have allowed researchers to gain unprecedented chemical and structural data on interfaces needed to improve corrosion models, which have in fact contradicted the majority of previous studies on both mineral and glass alteration mechanisms.

4.2. Dissolution/reprecipitation

Even though coupled interfacial dissolution-reprecipitation (CIDR) is a relatively recent theory as applied to glass corrosion, it traces its roots back to at least 1967, when it was proposed to explain the replacement of Na-feldspar by K-feldspar under hydrothermal conditions. Rather than invoking the standard idea of interdiffusional coupling of $Na^{+}_{feldspar} \leftrightarrow K^{+}_{solution}$ to explain the formation of authigenic K-feldspar, O'Neil and Taylor [28] instead postulated that "the mechanism of oxygen and cation exchange in these experiments involves the fine-scale solution and redeposition in a fluid film at the interface between the exchanged and unexchanged feldspar." Hay and Iijima [29] perhaps alluded to a similar process, "The sharp interface between unaltered sideromelane [a basaltic glass, see Ch. 7.2] and palagonite suggests that palagonite was formed by a microsolution-precipitation mechanism rather than by simple hydration and devitrification." In the following years, however, this new idea was to receive scant attention in the geosciences, or other related fields, for that matter.

Further development of the theory has been marked by an intertwined history between mineral and glass studies. At least 20 years ago, researchers primarily from the geochemical-mineralogical

community began to question the fundamental tenets of the traditional leached-layer model when novel experimental/analytical approaches were developed and applied to altered samples. These led to new interfacial measurements that ultimately made this change in *status quo* thinking possible. Thus, it took about 30 years after the publication of the pioneering O'Neil and Taylor study [28] for CIDR to be resurrected and further developed into a more complete theory for both mineral alteration [22,30] and glass corrosion [21,25,27].

According to the CIDR mechanism, the surface-altered layer (*i.e.*, equivalent to the interdiffusion zone and gel in Fig. 2) is essentially a precipitate of amorphous hydrated silica. In a superficial sense, this model resembles that of Fig. 1a, which was based on precipitation of crystalline (silicate) phases from an oversaturated bulk solution. The major difference is that the *coupled interfacial* dissolution-reprecipitation mechanism is based on an interfacial process involving tight spatial and temporal coupling between stoichiometric dissolution at a sharp chemical reaction front at the pristine glass surface, and quasi-simultaneous reprecipitation within an ultrathin fluid film in contact with the same interface. In cross section, this interfacial fluid film is composed of two to three ordered water molecules (< 1.3 nm in thickness) whose physical, chemical and rheological properties differ from those of bulk water [31,32]. These differences are postulated to make the precipitation of a secondary silica-rich phase on the glass surface possible, even when the bulk solution is completely undersaturated with respect to all silica polymorphs (*e.g.*, [25,27]).

With the CIDR mechanism, glass corrosion is initiated by local chemical disequilibrium between the pristine glass surface and the ordered water molecules of an interfacial fluid film (Fig. 6a), which results in hydrolysis reactions and the creation of a sharp dissolution front. The dissolution front is characterized by the stoichiometric release of the glass constituents into the fluid film. This process eventually leads to *interfacial* supersaturation within the fluid film, causing insoluble phases to precipitate (Fig. 6b). Dissolution and reprecipitation are nearly synchronous and spatially coupled within the interfacial fluid film. The predominant phase that generally precipitates is hydrated amorphous silica, but other insoluble metal oxyhydroxides (Fe, Al, Mo, etc.) may co-precipitate (at lesser concentrations) when these metals are present in the original glass structure. On the other hand, soluble cations, such as alkalis and alkaline earths, as well as boron, have only a minimal concentration in the reprecipitated layer through which they diffuse rapidly to the bulk

fluid. In fact, the relative degree of retention of elements released from the glass structure in the altered layer is largely controlled by thermodynamics (*i.e.*, by relative solubilities).

The thickness of the reprecipitated layer of silica increases with time, and depends on the net balance between dissolution-(re)precipitation processes at both the outer and inner interfaces of the surface-altered layer. Whereas the dynamics of the inner interface are controlled by the interfacial fluid, at the external interface they are controlled by the bulk fluid chemistry. An important aspect of the CIDR mechanism is that there is a net molar deficit for the overall reaction, which means that more moles of material are dissolved at the glass reaction front than are precipitated in the silica-rich surface-altered layer. As a result, the reprecipitate is quite porous [30], which allows for the unimpeded inward and outward flux of chemical entities (dissolution products, water and reactants from the bulk solution) between the reaction front at the glass surface and the bulk fluid. This is indicated in Fig. 6b by the arrows connecting the bulk fluid with the interfacial film. The precipitation of loosely packed silica spherules in glass corrosion layers [26] is supporting evidence for intrinsically high porosity and permeability. Pore size modification or even closure within the altered layer can occur over time [16]. Porous aggregates of secondary crystalline phases (zeolites, hydrosilicates, phyllosilicates, metal-oxyhydroxides [9,15]) may also crystallize from the bulk fluid on top of the surface-altered layer, depending on glass, bulk fluid and alteration conditions.

Perhaps the most important characteristic of CIDR is that the structural and chemical interfaces between the pristine glass and the reprecipitated silica are both very sharp and spatially commensurate at the nm-scale: in other words, they are the same interface. This would be expected for a precipitated phase in contact with an underlying parent phase. Evidence for such sharp and spatially coincident structural and chemical interfaces has recently been provided for a borosilicate glass altered in deionized water for 4 days and 1, 3 and 7 months [27]. In a series of STEM-HAADF and EFTEM images (Fig. 7), the surface-altered layer grows in thickness with time, and the boundary between the altered layer and the pristine glass remains very sharp at the nm-scale. In addition, the EFTEM chemical maps show that the altered layer is depleted in boron and enriched in silicon compared to the pristine glass and, most importantly, the chemical interface is also very sharp.

In that study [27], the 1-month corroded glass was also analyzed by APT to obtain 3-d distributions of cations in the altered layer and in the pristine glass. In a 2-d view of two of these reconstructions (Fig. 8a) the most interesting feature is the astounding sharpness of the chemical interface between the B and Ca-depleted altered layer and the unaltered glass. The abrupt nature of the structural and chemical interfaces (Figs. 7-8) is strong evidence in support of CIDR, but stands completely at odds with the leached-layer interdiffusion mechanism. Moreover, the depths of depletion or enrichment for 7 cations measured by APT are all equal (≈ 50 nm, Fig. 8b), even though these diverse cations carry charges ranging from +1 to +4. One of the tenets of diffusion is that cations diffuse at rates that vary inversely with charge (*e.g.*, Ch. 4.3, and the diffusion profiles of ref. [19])- but this is clearly violated by the results in [27]. It is also interesting to note that covalently bonded elements (network formers, *e.g.*, Si, O, Al, B) and more weakly bonded elements (network modifying cations, *e.g.*, Na, Li, Ca) show identical depths of depletion (Fig. 8b), despite their fundamentally different structural roles in the glass. Taken together, these results refute a diffusion mechanism. Other recent research also supports a non-traditional view of the corrosion process, or more precisely, the CIDR mechanism. In a recent isotope study [26], grains of a Na borosilicate glass enriched in ^{30}Si (^{28}Si/^{30}Si = 5-8) were altered in an aqueous solution in contact with a glass powder with a standard ratio of ^{28}Si/^{30}Si = 29.752. A solution labeled with ^{18}O was used either for the entire experiment, or was added halfway through it. The resulting ^{18}O/^{16}O and ^{28}Si/^{30}Si isotopic profiles not only differ in the altered layer and the glass, but include rhythmic patterns and multiple peaks of enrichment as a function of depth (Fig. 9). The Na profiles, on the other hand, revealed for the most part smooth depletion profiles, which might have resulted from the limited spatial resolution of the analyses. The textural interface between the surface altered layer and the pristine glass was sharp and characterized by chains of large pores. Finally, the altered layer showed evidence of spalling and flaking, indicative of very weak adherence (*i.e.*, bonding) to the pristine glass substrate- this would be expected for a mechanism based on reprecipitation. In an earlier study of borosilicate glass corrosion [25] the textural and chemical data were also completely at odds with the traditional mechanism in spite of the rather aggressive conditions of the experiments (initial pH ≈ 0, T = 150 °C). In the same study, a 2500-year old naturally altered glass from an archeological site revealed a

repetitive banding pattern in the corrosion rim, which quite closely resembles the chemical profiles obtained on the laboratory-altered glass [25].

4.3. *Pending questions*

Recent evidence [25-27] strongly supports the CIDR mechanistic framework of glass corrosion, which is also consistent with the APT-measured chemical profiles in Fig. 4a,b [6]. Nonetheless, the study of glass corrosion mechanisms remains controversial so that the CIDR mechanism is far from being universally accepted. One reason is the hypothesis of congruent dissolution at the glass surface reaction front; in particular, the idea that labile atoms, in particular network-modifier (or charge-compensating) cations, should be released at the same rate as covalently bonded framework-forming elements, which is perhaps counterintuitive. The CIDR model, however, does not exclude preferential ion exchange of cations with a fluid [22], as long as this process is restricted to labile atoms bonded at the *immediate* surface of the glass or mineral structure. The model does effectively preclude preferential ion exchange/release occurring deeper within the structure and the concomitant creation of a leached layer, which would invoke the (too) slow inward diffusion of reactants from the fluid. The exact mechanism of cation retention in the amorphous silica layer also merits more research. It is not known at present whether this occurs solely by co-precipitation with silica, or alternatively, by local precipitation of metal cation-oxyhydroxide phases within the nanopores of the silica layer. Cation adsorption on pore walls is another possible process. In fact, it is quite likely that all three processes occur during corrosion by CIDR.

The representation of a continuous fluid film contacting the pristine glass (Fig. 6) may require refinement. This idea stems from numerous studies that have shown that altered layers are loosely bound, or even physically separated from the underlying glass [19,26], resulting in facile detachment. On the other hand, not all studies have found evidence for spalling of the altered layer from the glass, suggesting stronger bonding. The interface might be more realistically characterized in terms of a dynamic island-fluid structure, as evidenced by chains of pores at the glass-altered layer interface [26]. Understanding the atomic nature of the interface and bonding between the altered layer and substrate glass, as well as the continuity of the fluid film, will require additional research. In particular, the use of aberration-corrected ultra high-resolution TEM applied to glass-

altered layer interfaces may be one key to understand better how they evolve. Liquid-cell TEM (LCTEM) also shows promise as a frontier technique, as it makes possible the study of aqueous alteration of minerals and glasses in situ and in real time [33].

The above questions will need to be addressed in more detail in the future as CIDR is further refined. Whether or not CIDR is a universal corrosion mechanism also remains an open question, which can only be answered with more research based on cutting edge analytical techniques applied to new samples, or even to samples previously studied.

5. Rates of dissolution and element release

5.1. Dissolution rates and how they are measured

Aqueous dissolution data, and in particular dissolution rates, are a valuable complement to solid-state data in determining the mechanism of dissolution. The overall, average long-term corrosion of glasses in aqueous fluids can be quantified in terms of total mass loss, normalized to surface area and elapsed time. However, in laboratory experiments, a far more useful quantification of corrosion is based on instantaneous rates of dissolution determined at specific time intervals. In a static reactor, the instantaneous release rate for any element i is defined as $R_i = \mathrm{d}c_i/\mathrm{d}t$; with units of $\mathrm{moles}_{(i)}\ \mathrm{m}^{-2}\ \mathrm{s}^{-1}$. When a continuous flow-through reactor is used, the concentration of an element i measured at any given time is directly proportional to its release rate. Individual elemental release rates always need to be normalized with respect to the compositional stoichiometry of the pristine glass. Corrosion rates are commonly reported in terms of framework elements such as Si or B, depending on the type of glass undergoing corrosion.

The two mechanistic models presented in Parts 3 and 4 differ in terms of where Si release occurs. With respect to the leached layer model, Si released to the bulk solution originates from the external interface of the gel layer and/or the diffusion zone (Figs. 2,3). In the CIDR model, Si also has two possible sources: the fraction of Si released from the pristine glass within the thin fluid film that is not precipitated diffuses directly through the altered layer to the bulk solution; the other Si source is the external interface of the silica-rich altered layer in contact with the bulk solution (Fig. 6b). In both models, the partitioning of Si release between their two respective sources is controlled in large part by the conditions of corrosion as well as the reaction progress variable.

5.2. Stoichiometry of dissolution rates

Glass dissolution kinetics can be quantified in terms of rates of release of network-forming cations, or alternatively, in terms of major elements present in the glass, irrespective of their structural role (*i.e.*, network-forming or -modifying cations). The stoichiometry of glass corrosion is frequently reported in terms of individual cationic release rates. In acidic and circumneutral pH solutions, the normalized cation concentrations in the bulk solution are in general not equal (i.e., non-stoichiometric) when plotted as a function of time (Fig. 10). Proponents of the leached-layer theory have used non-stoichiometric release rates as evidence for preferential release of certain labile elements coupled to incorporation of hydronium ions from the bulk solution. This is manifested by higher apparent release rates compared with that of Si, which ultimately results in the creation of a relict Si-rich leached layer (Figs. 1-3). However, the aqueous data purportedly showing preferential release can alternatively be explained in terms of CIDR. In this case the intrinsic dissolution process at the pristine glass surface is congruent, but subsequent retention (*i.e.*, reprecipitation) of released elements is controlled by each cation's relative solubility in the interfacial fluid film. Thus, soluble cations (Li, B) are preferentially released to the bulk solution, elements such as Cs with intermediate solubility are partially retained, and finally, minimally soluble elements (Si, Mo) are preferentially retained by the precipitation of an amorphous silica phase. Thus, the composition of the altered layer can be estimated by thermodynamics. The strong correlation between relative elemental solubility [34] and degree of retention within the altered layer (Fig. 10) is strong evidence in favor of CIDR, and not an interdiffusion-controlled leached layer process. This example also illustrates an important point: aqueous data alone, although useful, can be ambiguous, and therefore do not lend themselves to precise mechanistic interpretations. Thus, obtaining nanometer-scale solid-state data is primordial for the determination of any corrosion mechanism at the molecular scale.

As a final note, the aqueous data shown in Fig. 10 were used to calculate the Gibbs free energies (ΔG) of common low temperature polymorphs of silica (Supp. Info. [27]). All ΔG values were highly negative, thereby indicating that the observed amorphous Si-rich surface altered layers (Figs.

7-8) did not precipitate from an oversaturated bulk fluid, but more likely represent an interfacial reprecipitation phenomenon dependent on the special properties of thin fluid films.

5.3. Dissolution rates as a function of composition

Chemical composition is major factor in the corrosion of glasses. A classification of corrosion resistance of a broad range of compositions and types [35,36] shows the following generalized glass order (with some overlap between types): soda-lime (*e.g.*, medieval and antique glasses) < nuclear high-level waste (*e.g.*, SON68) < natural (*e.g.*, obsidian) < commercial (*e.g.*, Duran, Pyrex brands) < pure silica. A general rule of thumb is that corrosion durability increases with the proportion of network-forming elements (*e.g.*, Si, Al, B) coupled to a concomitant decrease in the abundance of network-modifying elements (*e.g.*, Ca, Na, Li, Mg, K). The former group of elements polymerizes the glass structure, whereas the latter depolymerizes it (Ch. 2.4).

To quantify these observations in terms of thermodynamics, many studies have used an approach based on a linear free energy relation (LFER). As developed in pioneering studies [37-38], the LEFR approach allows the susceptibility of glass to hydration (*i.e.*, aqueous corrosion) to be estimated from the weighted sum of the Gibbs free energies of hydration ($\Delta G_{hydr(i)}$) of its individual orthosilicate or oxide constituents (*i*). Although based on some restrictions and simplifying assumptions [35], this approach offers a good starting point for qualitatively estimating the durability of a glass. Thus, species such as SiO_2, Al_2O_3, CaO, Fe_2O_3 and MnO_2 are predicted to stabilize the glass structure (positive ΔG_{hydr} values), whereas $CaSiO_3$, Na_2SiO_3 and K_2SiO_3 destabilize it (negative ΔG_{hydr} values) [35]. There is, in fact, an inverse linear relation between log[Si] released and ΔG_{hydr} of the glass; in other words, the more negative ΔG_{hydr} , the less durable the glass and the higher the degree of Si release to solution. As a further refinement, ΔG_{hydr} can be adjusted for the solution pH to account for the dissociation of silicic and boric acids at high pH [36].

Glass composition is related to structure in terms of non-bonding oxygen (NBO) bonds, since ΔG_{hydr} correlates well with the number of NBO [37]. Hence, glass structure is usually not considered as a separate mesoscopic parameter distinct from composition. At the molecular scale it nonetheless plays a key role in glass corrosion, seemingly contradicting the preceding statement. As

an example [16], it was found that the initial corrosion rate of a borosilicate glass was slowed down by substitution of zirconia (0-8 mol % ZrO_2) for silica. In the long term, however, the overall degree of corrosion increased with zirconia concentration because ZrO_2 hindered restructuring of the gel layer and, thereby, prevented pore closure. This phenomenon was deduced to be ultimately responsible for stopping corrosion by drastically decreasing the rates of diffusion of aqueous species within the gel.

5.4. Dissolution rates as a function of pH and temperature

The effect of pH and temperature on glass dissolution is also quite strong, and is just as important as chemical composition of the glass. As has been developed and described in numerous geochemical studies for mineral dissolution kinetics, the following type of generalized rate equation for heterogeneous surface reactions [39] has also been widely applied to glass corrosion in aqueous solutions:

$$Rate = k_0 A e^{-E_a/RT}\, a_{H+}^{n_{H+}} \prod_i a_i^{ni}\, f(\Delta G_r) \qquad (1)$$

In eqn (1), k_0 is the forward rate constant, A the reactive surface area, E_a the thermal activation energy of the overall reaction, R the gas constant, and $a_{H+}^{n_{H+}}$ the activity of H^+ raised to a power n; the product operator term expresses the influence of the activities of other aqueous species that either catalyze or hinder the dissolution reaction; finally, $f(\Delta G_r)$ is a Gibbs free energy (or chemical affinity) term expressing the effect of deviation from chemical equilibrium on the rate, written here in a manner not based on any specific mechanism (*e.g.*, transition state theory). By definition, $f(\Delta G_r) = 0$ at equilibrium. Many of the parameters in eqn (1), such as k_0, n, E_a and $f(\Delta G_r)$, can vary as a function of temperature, pressure, pH, and other variables.

If corrosion takes place far from equilibrium, and catalysis/inhibition due to other species in solution is unimportant, then eqn (1) can be simplified and rewritten in terms of two equivalent expressions [39]:

$$Rate = k_0 A e^{-E_a/RT}\, a_{H+}^{n_{H+}} \quad (2a) \qquad Rate = k_0 A e^{-E_a/RT}\, X_{H+,\ ads}^{n_{H+,\ ads}} \quad (2b)$$

Whereas eqn (2a) expresses the pH dependence of corrosion in terms of the activity of H^+, eqn (2b) expresses it in terms of the mole fraction of H^+ adsorbed on surface sites. Both approaches are valid, but do not necessarily predict identical rates.

At any given temperature glass dissolution rates show a U- or V-shaped dependence on pH commonly observed for silicate minerals, which is not necessarily symmetric with respect to pH. As determined from regression of rate-pH data or adsorption isotherms of H^+ or OH^-, the values for *n* in eqns (1-2) generally range from 0 to 1 at acid pH and 0 to -1 at basic pH, where corrosion is catalyzed by H^+ and OH^-, respectively. At 4 < pH < 8, the pH dependence is weak at most, so that corrosion rates are more or less constant (over a pH range that may be more restricted). Activation energies, derived from regression of ln *R* vs 1/*T* (K) data, are typically around 80 kJ mol^{-1} [34]. They are representative of hydrolysis reactions of 3-d networks of cation-oxygen framework bonds. With respect to both the leached-layer model and CIDR, an E_a = 80 kJ mol^{-1} increases the (Si) release rate by a factor of 20 between 25 and 55 °C. However, advance of the diffusion front into the pristine glass (Fig. 2) is characterized by a significantly higher E_a, which reflects the extremely slow nature of solid-state diffusion at low to moderate temperatures [20].

5.5. Decrease of dissolution rates by chemical affinity (ΔG_r) and pore closure effects

A smooth exponential decrease of release rates is observed in virtually all glass corrosion studies (Fig. 10). In terms of leached layer theory, this evolution has been split into five regimes [7] that have no precise boundaries: (i) initial diffusion (interdiffusion); (ii) initial rate; (iii) rate drop; (iv) residual rate; (v) alteration resumption (only under certain conditions). The chemical and physical causes of the rate decrease have long been debated. In closed systems, a decrease of the $f(\Delta G_r)$ term in eqn (1) has been commonly invoked as a result of the increasing concentration of dissolved glass species (*i.e.*, Si) in solution. With the assumption of a rate-controlling activated-surface complex, Aagaard and Helgeson [40] calculated from transition-state theory that:

$$f(\Delta G_r) = \left[1 - \exp\left(n\frac{\Delta G_r}{RT}\right)\right] \qquad (3)$$

With *n* = 1 [39], eqn (3) can then be expressed in a simpler form:

$$f(\Delta G_r) = (1 - Q/K) \qquad (4)$$

Alternative relations have also been suggested, for instance

$$f(\Delta G_r) = (1 - (Q/K)^{1/n}) \qquad (5)$$

with *n* = 10 [41]. In both eqns (4) and (5), *Q* refers to the ion activity product (IAP) of a given dissolution reaction and *K* refers to the IAP at chemical equilibrium (*i.e.*, solubility product).

Application of such relations to glass corrosion is problematic because a glass and a solution cannot be in chemical equilibrium since the reverse reaction will not lead to glass precipitation. Defining the Q/K ratio with respect to glass corrosion has thus been very controversial.

According to Grambow [42], dissolution of borosilicate glasses can be represented by the reaction $SiO_2 + H_2O \Leftrightarrow H_4SiO_4$. This approach relies on the assumption $A_{glass} \approx A_{SiO2}$ (A denotes affinity), such that the parameter Q in eqn. (4) represents the aqueous silica concentration in the bulk solution and porous gel, and K refers to the solubility of amorphous SiO_2. At advanced reaction progress, the build up of aqueous silica in the bulk solution and within the pores of the gel will progressively slow down the release of Si from the external interface of the diffusion layer (Fig. 2). The original hypothesis of A_{SiO2}-controlled dissolution was subsequently modified to include the effect of water diffusion through the hydrated diffusion layer [11]: if the layer is thin and water diffusion is unhindered, corrosion can continue at elevated rates, even for chemical affinity conditions of the bulk solution close to silica saturation. The same study [11] also suggested that soluble elements (*e.g.*, Na and B) have a 'collective response' with respect to silica concentrations, meaning that their release rates decrease significantly when the bulk solution attains silica saturation.

Nonetheless, the silica-affinity model [42] has been criticized for not being compatible with many experimental observations [8]. Recent experiments on SON68 glass based on progressive addition of aqueous silica (0-150 ppm Si) have also cast doubt on its validity [43]. Even though rates decreased by a factor of 150 upon addition of Si, their pronounced non-linear nature stands at odds with the linear decrease predicted by eqn (4). In part because of such observations, a similar affinity model depending on the dissolution affinity of the gel layer was proposed [44]. Rather than just considering silica, it postulates that all elements in the solution and in the gel layer determine the dissolution affinity. This approach therefore predicts that long-term corrosion is controlled by the chemistry of the bulk solution, and in particular, by secondary phases which precipitate and thereby control ion concentrations.

Another viable mechanism accounting for decreasing reaction rates is based on the transport properties of surface altered layers. These layers have the potential to decrease the bidirectional fluxes of aqueous reactant and product species between the bulk solution and the pristine glass. Alteration layers that form upon corrosion may be intrinsically dense, or may morphologically

evolve with time so as to progressively decrease rates of diffusion of aqueous species within their porous structure. It has been argued that progressive densification of the outer parts of gel layers leads to pore closure [16], which in turn significantly decreases diffusion rates within the gel layer and thereby the intrinsic rate of glass dissolution. Another study used ^{29}Si isotope tracer profiles measured on two different sample faces after 86-day corrosion experiments [45]: from the outer gel edge to the gel-pristine glass interface, ^{29}Si diffused a total distance of 950 nm (bulk solution side); on the other side of the monolith in contact with a glass powder, the gel thickness was much thinner (≈ 150 nm), and most importantly, the gel acted as a diffusion barrier to ^{29}Si, allowing penetration only over the outermost 30 nm. For closure of gel porosity to occur, and by implication a corrosion rate that becomes negligible ($R \approx 0$), the authors [45] postulated that two conditions must be met: (i) the gel must have a high Si concentration; (ii) the bulk solution must be silica-saturated. Complementary Monte Carlo simulations supported these results and showed that clogging of the porous gel occurred at the external gel-bulk solution interface.

6. Perspectives

A systematic approach is needed to study in detail the molecular-scale mechanisms that control chemical alteration of glasses in aqueous solutions. This goal can only be achieved with a methodology that goes beyond standard analytical methods that have been widely used in the past. The choice of how altered glass samples are prepared, and which analytical techniques are used, is of critical importance for obtaining data useful in deciphering the molecular-scale mechanism of alteration, as well as modeling the glass corrosion process and its kinetics. Based on published data, the decrease in long-term rates of dissolution most likely are due to chemical and physical processes operating in tandem. More in-depth work will have to be done to ascertain the partitioning between chemical and physical rate-decreasing processes as a function of time during glass corrosion.

The cornerstone for the long-term prediction of glass corrosion is an accurate understanding of the underlying mechanism(s). Therefore, employing high-spatial and high mass-resolution techniques to analyze surface altered phases and their interfaces with unaltered glass should be strongly encouraged for future glass studies. Moreover, corrosion experiments using isotopically-labeled bulk fluids, and in some cases even labeled glasses, have already shown their enormous potential to

provide complementary information on the dynamics of glass corrosion. When taken together, the combined use of all of these advanced techniques may allow for a long-term goal to be realized: establishing whether or not all glasses are ultimately controlled by the same mechanism of dissolution. Going even further, it may perhaps even lead to a universal mechanism that links mineral and glass alteration processes at the nm-scale.

Index terms:
leached layer, leached layer-interdiffusion mechanism, coupled interfacial dissolution-reprecipitation mechanism (CIDR), palagonite, gel, surface altered layer, hydrated layer, authigenic mineral, abiotic corrosion, volcanic basalt glass, borosilicate glass, SON68 nuclear analog glass, isotopic labeling

Acknowledgements

The author thanks the reviewers J.P. Icenhower, T. Geisler, and E. Ruiz-Agudo (Dept. Mineralogy and Petrology, Univ. Granada, Spain) for their useful comments and suggestions.

References

1. H. Staudigel, Chemical fluxes from hydrothermal alteration of the oceanic crust, p. 583-606 in H.D. Holland and K.K. Turekian (eds), *Treatise on Geochemistry* (Amsterdam: Elsevier, 2013, 2nd ed.).

2. B. Grambow, Nuclear waste glasses - how durable? *Elements*, 2 (2006) 357-364.

3. L. M. Anovitz, J. M. Elam, L. R. Riciputi and D. R. Cole, The failure of obsidian hydration dating: Sources, implications, and new directions, *J. Archeol. Sci.*, 26 (1999) 735-52.

4. J.-C. Dran, J.-C. Petit and C. Brouse, Mechanism of aqueous dissolution of silicate glasses yielded by fission tracks, *Nature*, 319 (1986) 485-87.

5. J.-L. Crovisier, T. Advocat and J.-L. Dussossoy, Nature and role of natural alteration gels formed on the surface of ancient volcanic glasses (Natural analogs of waste containment glasses), *J. Nucl. Mater.*, 321 (2003) 91-109.

6. S. Gin, J. V. Ryan, D. K. Schreiber, J. Neeway and M. Cabié, Contribution of atom-probe tomography to a better understanding of glass alteration mechanisms: Application to a nuclear glass specimen altered 25 years in a granitic environment, *Chem. Geol.*, 349-350 (2013) 99-109.

7. P. Frugier *et al.*, SON68 nuclear glass dissolution kinetics: Current state of knowledge and basis of the new GRAAL model, *J. Nucl. Mater.*, 380 (2008) 8-21.

8. C. Jégou, S. Gin and F. Larché, Alteration kinetics of a simplified nuclear glass in an aqueous medium: effects of solution chemistry and of protective gel properties on diminishing the alteration rate, *J. Nucl. Mater.*, 280 (2000) 216-29.

9. N. Valle, A. Verney-Carron, J. Sterpenich, G. Libourel, E. Deloule, and P. Jollivet, Elemental and isotopic (^{29}Si and ^{18}O) tracing of glass alteration mechanisms, *Geochim. Cosmochim. Acta.*, 74 (2010) 3412-31.

10. R. H. Doremus, Interdiffusion of hydrogen and alkali ions in a glass surface, *J. Non-Cryst. Solids*, 19 (1975) 137-44.

11. B. Grambow and R. Müller, First-order dissolution rate law and the role of surface layers in glass performance assessment, *J. Nucl. Mater.*, 298 (2001) 112-24.

12. J.-C. Dran, G. Della Mea, A. Paccagnella, J.-C. Petit and L. Trotignon, The aqueous dissolution of alkali silicate glasses: reappraisal of mechanisms by H and Na depth profiling with high energy ion beams, *Phys. Chem. Glasses*, 29 (1988) 249-55.

13. J.-C. Petit, G. Della Mea, J.-C. Dran, M.-C. Magonthier, P. A. Mando and A. Paccagnella, Hydrated layer formation during dissolution of complex silicate glasses and minerals, *Geochim. Cosmochim. Acta*, 54 (1990) 1941-55.

14. B. C. Bunker, Molecular mechanisms for corrosion of silica and silicate glasses, *J. Non-Cryst. Solids*, 179 (1994) 300-08.

15. J.-H. Thomassin, F. Boutonnat, J.-C. Touray and P. Baillif, Geochemical role of the water/rock ratio during the experimental alteration of a synthetic basaltic glass at 50°C. An XPS and STEM investigation, *Eur. J. Mineral.*, 1 (1989) 261-74.

16. C. Cailleteau *et al*., Insight into silicate-glass corrosion mechanisms, *Nature Mater.*, 7 (2008) 978-983.

17. H. Staudigel, H. Furnes, N. McLoughlin, N. R. Banerjee, L. B. Connell and A. Templeton, 3.5 billion years of glass bioalteration: Volcanic rocks as a basis for microbial life? *Earth-Sci. Rev.*, 89 (2008) 156-76.

18. R. Hellmann, The albite-water system Part IV. Diffusion modeling of leached and hydrogen-enriched layers, *Geochim. Cosmochim. Acta*, 61 (1997) 1595-1611.

19. R. Hellmann *et al.*, Unifying natural and laboratory chemical weathering with interfacial dissolution–reprecipitation: A study based on the nanometer-scale chemistry of fluid–silicate interfaces, *Chem. Geol.*, 294-295 (2012) 203-16.

20. I. M. Vila, Diffusion in mineral geochronometers: Present and absent, *Chem. Geol*., 420 (2016) 1-10.

21. E. C. Buck, K. L. Smith and M. G. Blackford, The behavior of silicon and boron in the surface of corroded nuclear waste glasses: an EFTEM study, *Mat. Res. Soc. Symp. Proc.*, 608 (2000) 727-32.

22. R. Hellmann, J.-M. Penisson, R. L. Hervig, J.-H. Thomassin and M.-F. Abrioux, An EFTEM/HRTEM high-resolution study of the near surface of labradorite feldspar altered at acid pH: evidence for interfacial dissolution-reprecipitation, *Phys. Chem. Miner.*, 30 (2003) 192-97.

23. R. Wirth, Focused Ion Beam (FIB): A novel technology for advanced application of micro- and nanoanalysis in geosciences and applied mineralogy, *Eur. J. Mineral*., 16 (2004) 863-76.

24. D. Daval *et al*., Influence of amorphous silica layer formation on the dissolution rate of olivine at 90°C

and high pCO_2, *Chem. Geol.*, 284 (2011) 193-209.

25. T. Geisler, A. Janssen, D. Scheiter, T. Stephan, J. Berndt and A. Putnis, Aqueous corrosion of borosilicate glass under acidic conditions: A new corrosion mechanism, *J. Non-Cryst. Solids*, 356 (2010) 1458-65.

26. T. Geisler *et al.*, The mechanism of borosilicate glass corrosion revisited, *Geochim. Cosmochim. Acta*, 158 (2015) 112–129.

27. R. Hellmann *et al*., Nanometre-scale evidence for interfacial dissolution–reprecipitation control of silicate glass corrosion, *Nature Mater*., 14 (2015) 307-11.

28. J. R. O'Neil and H. P. J. Taylor, The oxygen isotope and cation exchange chemistry of feldspars, *Amer. Mineral.*, 52 (1967) 1414-37.

29. R. L. Hay and A. Iijima, Nature and origin of palagonite tuffs of the Honolulu Group, on Oahu, Hawaii, in Studies in Volcanology: A Memoir in Honor of Howell Williams, *Mem. Geol. Soc. Amer*., 116 (1968) 331–76.

30. A. Putnis, Mineral replacement reactions: from macroscopic observations to microscopic mechanisms, *Mineral. Mag*., 66 (2002) 689-708.

31. P. Fenter and N. C. Sturchio, Mineral-water interfacial structures revealed by synchrotron X-ray scattering, *Prog. Surf. Sci.*, 77 (2004) 171-258.

32. V. Marry, B. Rotenberg and P. Turq, Structure and dynamics of water at a clay surface from molecular dynamics simulation, *Phys. Chem. Chem. Phys.*, 10 (2008) 4802–13.

33. D. Leonard and R. Hellmann, Exploring dynamic surface processes during silicate mineral dissolution with liquid cell TEM, *J. Micros.*, 265 (2017) 358-71.

34. R. Conradt, Chemical durability of oxide glasses in aqueous solutions: a review, *J. Amer. Ceram. Soc*., 91 (2008) 728-35.

35. D. Perret *et al.*, Thermodynamic stability of waste glasses compared to leaching behaviour. *Appl. Geochem.* 18 (2003) 1165-84.

36. C. M. Jantzen, Prediction of glass durability as a function of glass composition and test conditions: thermodynamics and kinetics, p. 24.1–24.17 in D. F. Bickford *et al.*, (eds), *Proc. 1st Int. Conf. Advances Fusion Glass* (1988).

37. A. Paul, *Chemistry of Glasses* (London: Chapman & Hall, 1982).

38. C. M. Jantzen and M. J. Plodinec, Thermodynamic model of natural, medieval and nuclear waste glass durability, *J. Non-Cryst. Solids*, 67 (1984) 207-23.

39. A. C. Lasaga, J. M. Soler, J. Ganor, T. E. Burch, and K. L. Nagy, Chemical weathering rate laws and global geochemical cycles, *Geochim. Cosmochim. Acta*, 58 (1994) 2361-86.

40. P. Aagaard and H. C. Helgeson, Thermodynamic and kinetic constraints on reaction rates among minerals and aqueous solutions. I. Theoretical considerations, *Amer. J. Sci.*, 282 (1982) 237-85.

41. W. H. Bourcier, S. A. Carroll, and B. L. Phillips, Constraints on the affinity term for modeling long-term glass dissolution rates, *Mat. Res. Soc. Symp. Proc.*, 333 (1994) 507-512.

42. B. Grambow, A general rate equation for nuclear waste glass corrosion, *Mater. Res. Soc. Symp. Proc*., 44 (1985) 15–27.

43. J.P. Icenhower and C.I. Steefel, Experimentally determined dissolution kinetics of SON68 glass at 90 °C over a silica saturation interval: Evidence against a linear rate law, *J. Nucl. Mater*., 439 (2013) 137-47.

44. W. L. Bourcier, D. W. Pfeiffer, K. G. Knauss, K. D. McKeegan, and D. K. Smith, A kinetic model for borosilicate glass dissolution based on the dissolution affinity of a surface alteration layer, *Mat. Res. Soc. Symp. Proc.*, 176 (1990) 209-16.

45. P. Jollivet, F. Angeli, C. Cailleteau, F. Devreux, P. Frugier, and S. Gin, Investigation of gel porosity clogging during glass leaching, *J. Non-Cryst. Solids*, 354 (2008) 4952-58.

Table 1. Chemical-gradient widths (nm) of boron profiles in surface altered layers formed on SON68 borosilicate glass measured with different techniques [6]

ToF-SIMS	>1000
nanoSIMS (O^- beam)	350 ± 150
nanoSIMS (Cs^+ beam)	170 ± 30
EFTEM	≤ 30
APT	3-4

Figure Captions

Fig. 1. Cross sectional diagrams of early models of an altered glass layer. (a) Congruent glass dissolution, followed by precipitation of secondary crystalline phases on the glass surface from a saturated solution. (b) *In situ* transformation of the glass structure via selective cation removal by interdiffusion, characterized by sigmoidal and anti-correlated H and cation depth profiles.

Fig. 2. The distinct chemistry and structure of the three layers of the leached layer mechanism: anti-correlated chemical profiles in the interdiffusion zone, relatively constant concentrations in the amorphous gel phase, and specific compositions of crystalline precipitates at the interface between the gel and the corroding aqueous solution.

Fig. 3. The interdiffusion zone, gel and surficial crystalline phases of the leached layer model illustrated by chemical profiles measured after a 3-month corrosion of SON68 borosilicate glass at 90 °C and pH 8. SIMS O^- ion beam rastered over 250 x 250 μm^2 area, positive ions collected from window covering 60% of this area. Adapted from Fig. 6, [9].

Fig. 4. Chemical profiles of pristine glass-hydrated glass interface obtained by atom probe tomography (APT) of a borosilicate SON68 sample corroded 25.75 years at 90 °C and pH 7. (a) Profiles extending from the pristine glass to a depth of 500 nm into the hydrated glass. (b) Close up of the first 30 nm of the hydrated glass, based on original profiles (a) that were replotted with a 'proximity histogram method', producing significantly sharper elemental gradient widths. The true [B] may be lower than shown- see [6]. Adapted from Fig. 3, [6].

Fig. 5. Hybrid leached layer-preferential dissolution model [6] illustrated by a schematic partial cross section of the hydrated layer and its two interfaces (refer to previous Fig. 4). (a) The 1000-nm thick hydrated glass (interdiffusion) layer is shown in its entirety. The sharp interdiffusion profiles and preferential dissolution front occupy only the extremity of the hydrated glass layer, at the inner

interface with the pristine glass (20-nm thick light vertical band, drawn to scale). (b) Close up of inner interfacial region, showing partially overlapping profiles representing interdiffusion (H and Li), preferential dissolution (Na, B), and diffusive uptake (K) from the bulk solution.

Fig. 6. Glass corrosion by coupled interfacial dissolution-reprecipitation (CIDR). (a) Initial stage: congruent glass dissolution in a thin fluid film comprised of 2 to 3 ordered H_2O molecules. (b) Advanced stage: pristine glass, thin fluid film, reprecipitated layer primarily composed of hydrated amorphous silica, surficial secondary crystalline phases, and bulk solution. Soluble cations (B, alkalis and alkaline earth elements) diffuse unhindered to the bulk solution through the porous altered layer.

Fig. 7. Corrosion of SON68 borosilicate glass altered at 50°C in water for increasing periods of time. On left, STEM-HAADF images of the corrosion front, the surface altered layer is delimited by arrows (scale bar: 25 nm). Center and right : EFTEM maps of boron and silicon, respectively, showing B depletion and Si enrichment (scale bar: 100 nm). In each panel, C denotes carbon (from sample preparation). Cross sections prepared either by FIB milling or Ar ion thinning. Adapted from Fig. 1, [27].

Fig. 8. Chemical evolution of SON68 borosilicate glass after one month of corrosion measured by atom probe tomography. (a) APT reconstruction of almost atomically sharp interface between the 50-nm thick B and Ca-depleted surface altered layer and unaltered glass (each dot represents an atom). (b) Chemical profiles across glass-altered layer interface based on 3-d APT reconstructions: note sharp concentration drops of B, Li, Ca, and Na and corresponding sharp increases in Si, Al and O at interfacial boundary. Monotonous increases in Li and Na after initial jumps due to thermal diffusion during laser pulsing. Profiles at -20 nm, from high to low concentration: O, Si, Al, B, Ca, Na, Li. From Fig. 2, [27].

Fig. 9. Complex chemical patterns and prevalent µm-sized porosity of silica-rich alteration layers formed during corrosion of a borosilicate glass: nanoSIMS intensity images of ^{16}O (a-c), $^{18}O/^{16}O$ (d-f), and $^{28}Si/^{30}Si$ (g-i) of glass grains enriched in ^{30}Si and reacted in ^{18}O-labeled solutions containing a glass powder with a standard $^{28}Si/^{30}Si$ ratio. Conditions: 672 hours, 90 °C, pH = 9.6. Reprinted with permission: Fig. 3, [29].

Fig. 10. Aqueous elemental release curves as a function of time measured during corrosion of SON68 glass. The non-stoichiometry of the normalized elemental release rates ($R_{Li} \approx R_B > R_{Cs} > R_{Si} \approx R_{Mo}$) was attributed to solubility control (*i.e.*, CIDR) within thin fluid film at pristine glass dissolution front. These data complement solid-state results for the 1-month sample shown in Figs. 7-8. Adapted from Fig. S4, Supp. Information, [27].

Fig. 1. Cross sectional diagrams of early models of an altered glass layer. (a) Congruent glass dissolution, followed by precipitation of secondary crystalline phases on the glass surface from a saturated solution. (b) *In situ* transformation of the glass structure via selective cation removal by interdiffusion, characterized by sigmoidal and anti-correlated H and cation depth profiles.

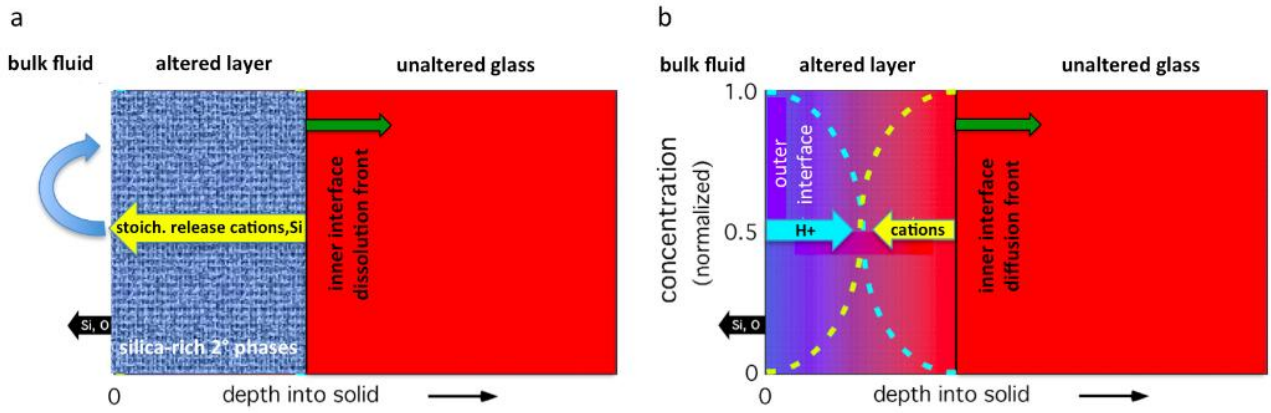

Fig. 2. The distinct chemistry and structure of the three layers of the leached layer mechanism: anti-correlated chemical profiles in the interdiffusion zone, relatively constant concentrations in the amorphous gel phase, and specific compositions of crystalline precipitates at the interface between the gel and the corroding aqueous solution.

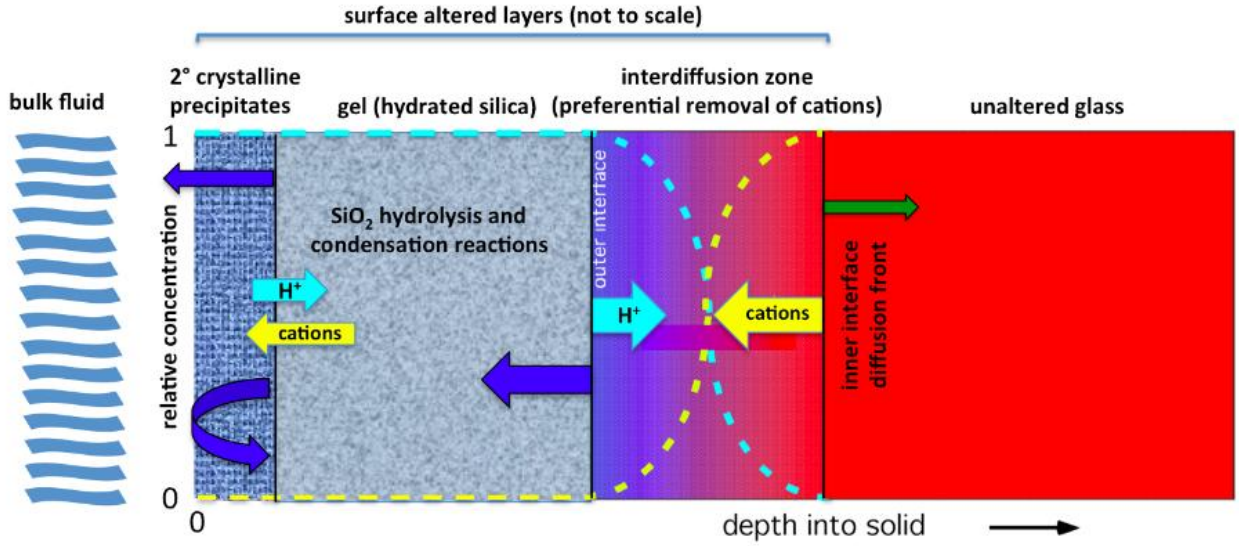

Fig. 3. The interdiffusion zone, gel and surficial crystalline phases of the leached layer model illustrated by chemical profiles measured after a 3-month corrosion of SON68 borosilicate glass at 90 °C and pH 8. SIMS O^- ion beam rastered over 250 x 250 μm^2 area, positive ions collected from window covering 60% of this area. Adapted from Fig. 6, [9].

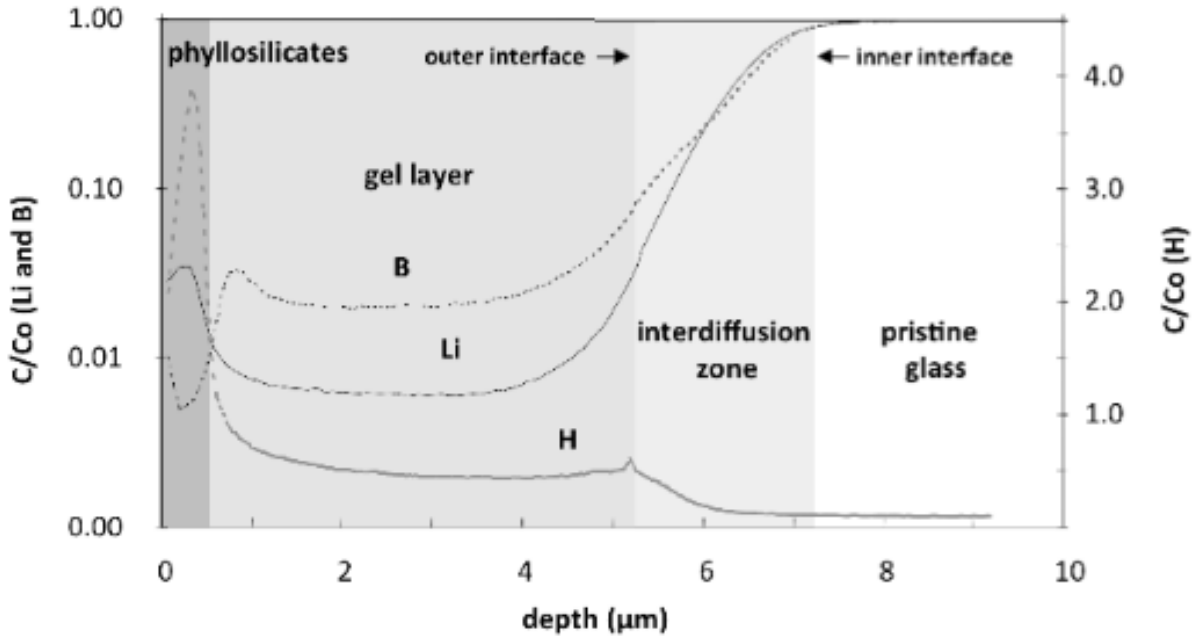

Fig. 4. Chemical profiles of pristine glass-hydrated glass interface obtained by atom probe tomography (APT) of a borosilicate SON68 sample corroded 25.75 years at 90 °C and pH 7. (a) Profiles extending from the pristine glass to a depth of 500 nm into the hydrated glass. (b) Close up of the first 30 nm of the hydrated glass, based on original profiles (a) that were replotted with a 'proximity histogram method', producing significantly sharper elemental gradient widths: Na and B (3-4 nm), K (5 nm), Li (17 nm) and H (20 nm). The true [B] may be lower than shown- see [6]. Adapted from Fig. 3, [6].

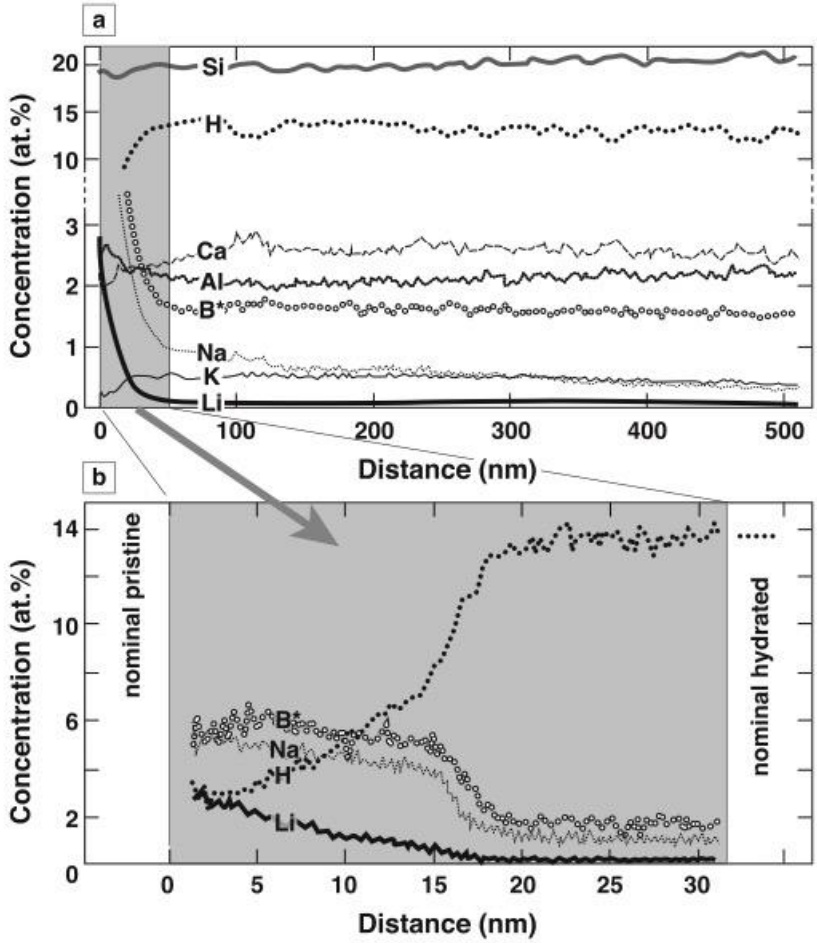

Fig. 5. Hybrid leached layer-preferential dissolution model [6] illustrated by a schematic partial cross section of the hydrated layer and its two interfaces (refer to previous Fig. 4). (a) The 1000-nm thick hydrated glass (interdiffusion) layer is shown in its entirety. The sharp interdiffusion profiles and preferential dissolution front occupy only the extremity of the hydrated glass layer, at the inner interface with the pristine glass (20-nm thick light vertical band, drawn to scale). (b) Close up of inner interfacial region, showing partially overlapping profiles representing interdiffusion (H and Li), preferential dissolution (Na, B), and diffusive uptake (K) from the bulk solution.

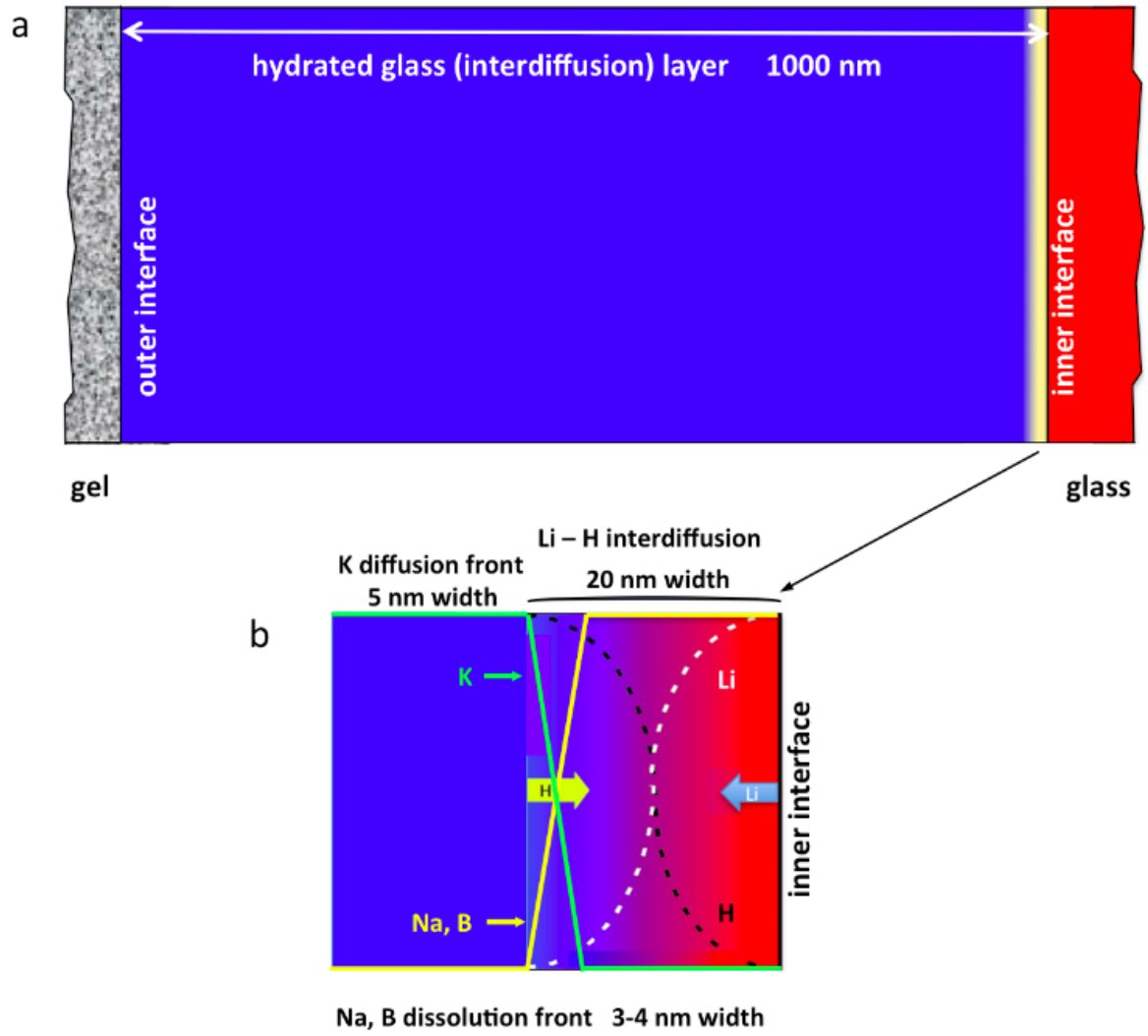

Fig. 6. Glass corrosion by coupled interfacial dissolution-reprecipitation (CIDR). (a) Initial stage: congruent glass dissolution in a thin fluid film comprised of 2 to 3 ordered H_2O molecules. (b) Advanced stage: pristine glass, thin fluid film, reprecipitated layer primarily composed of hydrated amorphous silica, surficial secondary crystalline phases, and bulk solution. Soluble cations (B, alkalis and alkaline earth elements) diffuse unhindered to the bulk solution through the porous altered layer.

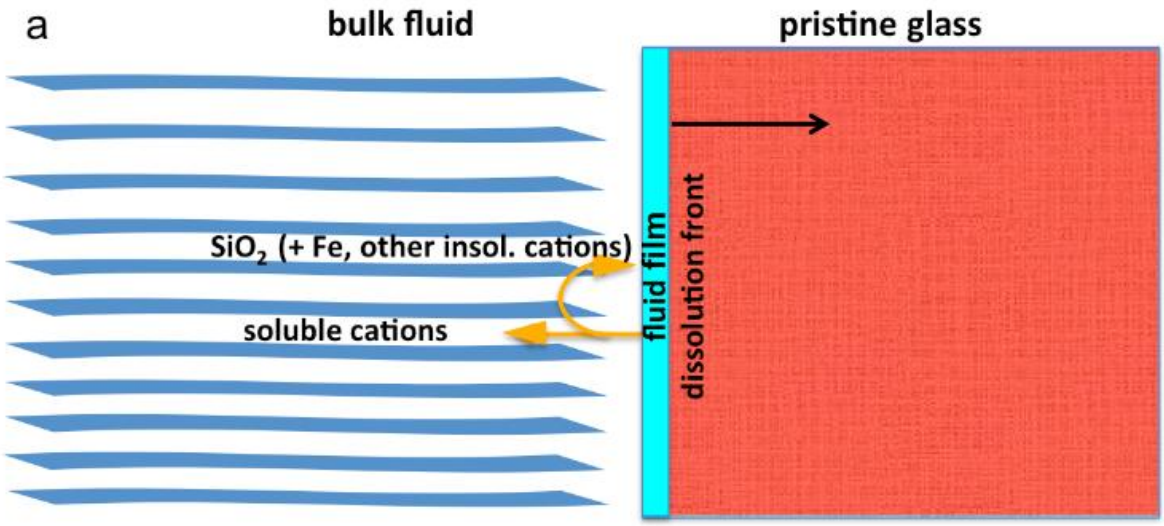

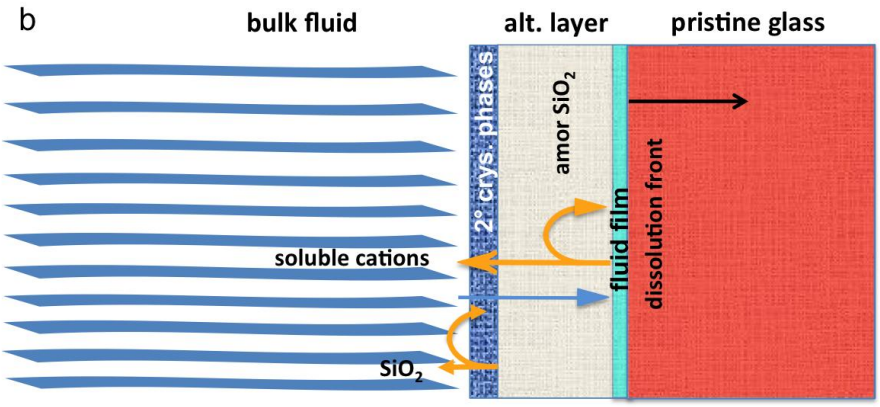
b
bulk fluid
alt. layer
pristine glass
2° crys. phases
amor SiO2
fluid film
dissolution front
soluble cations
SiO2

Fig. 7. Corrosion of SON68 borosilicate glass altered at 50°C in water for increasing periods of time. On left, STEM-HAADF images of the corrosion front, the surface altered layer is delimited by arrows (scale bar: 25 nm). Center and right : EFTEM maps of boron and silicon, respectively, showing B depletion and Si enrichment (scale bar: 100 nm). In each panel, C denotes carbon (from sample preparation). Cross sections prepared either by FIB milling or Ar ion thinning. Adapted from Fig. 1, [27].

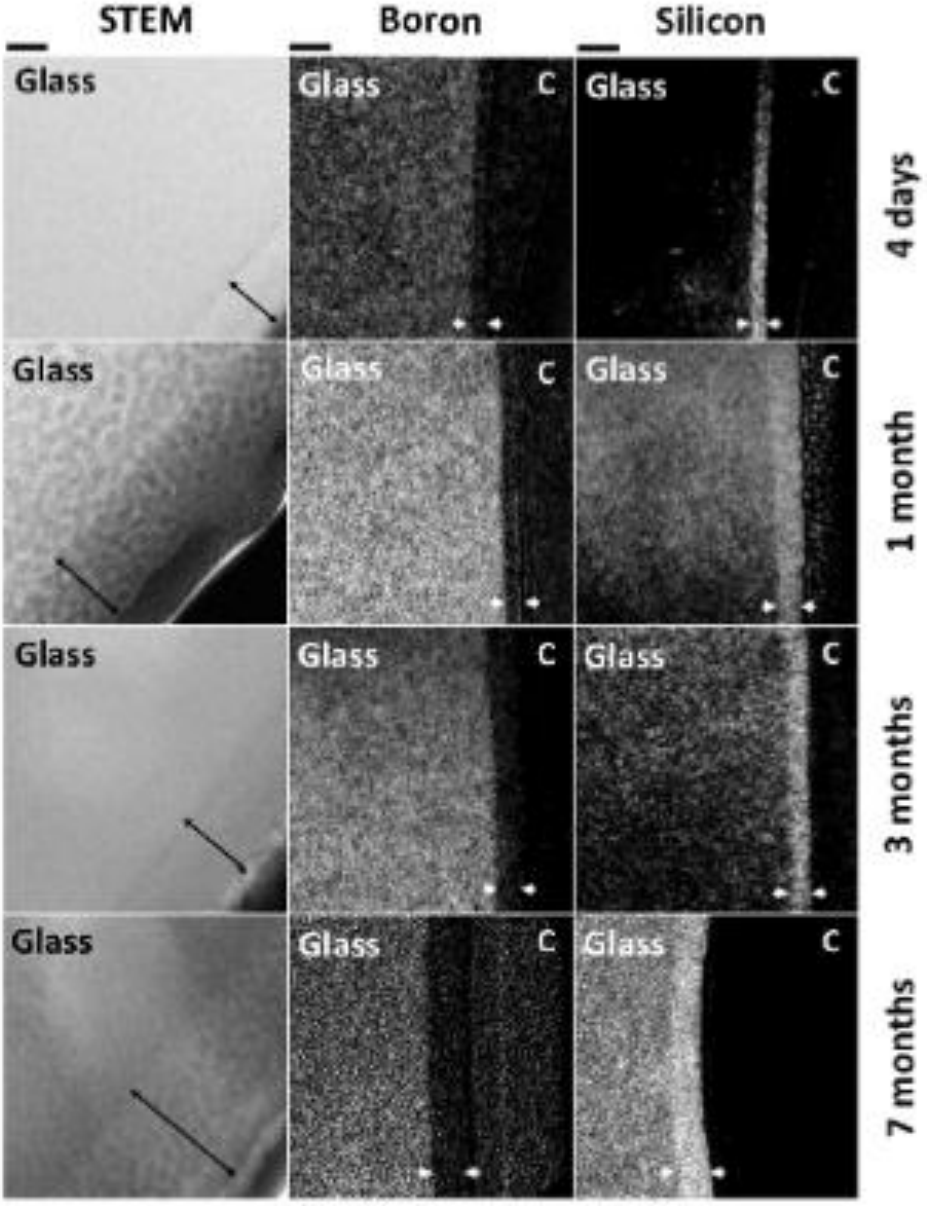

Fig. 8. Chemical evolution of SON68 borosilicate glass after one month of corrosion measured by atom probe tomography. (a) APT reconstruction of almost atomically sharp interface between the 50-nm thick B and Ca-depleted surface altered layer and unaltered glass (each dot represents an atom). (b) Chemical profiles across glass-altered layer interface based on 3-d APT reconstructions: note sharp concentration drops of B, Li, Ca, and Na and corresponding sharp increases in Si, Al and O at interfacial boundary. Monotonous increases in Li and Na after initial jumps due to thermal diffusion during laser pulsing. Profiles at -20 nm, from high to low concentration: O, Si, Al, B, Ca, Na, Li. Adapted from Fig. 2, [27].

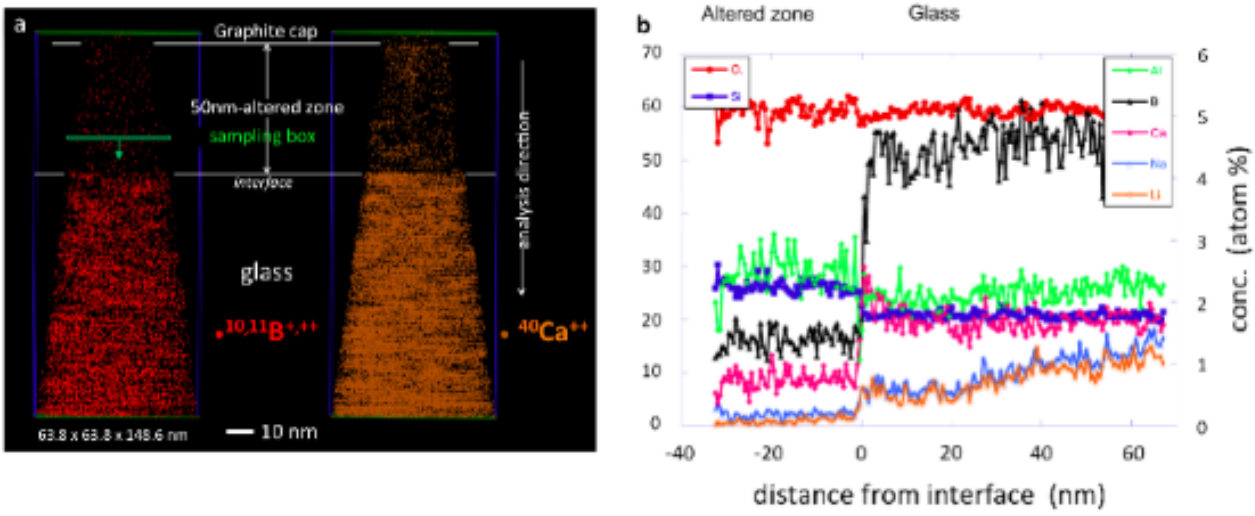

Fig. 9. Complex chemical patterns and prevalent µm-sized porosity of silica-rich alteration layers formed during corrosion of a borosilicate glass: nanoSIMS intensity images of ^{16}O (a-c), $^{18}O/^{16}O$ (d-f), and $^{28}Si/^{30}Si$ (g-i) of glass grains enriched in ^{30}Si and reacted in ^{18}O-labeled solutions containing a glass powder with a standard $^{28}Si/^{30}Si$ ratio. Conditions: 672 hours, 90 °C, pH = 9.6. Reprinted with permission: Fig. 3, [29].

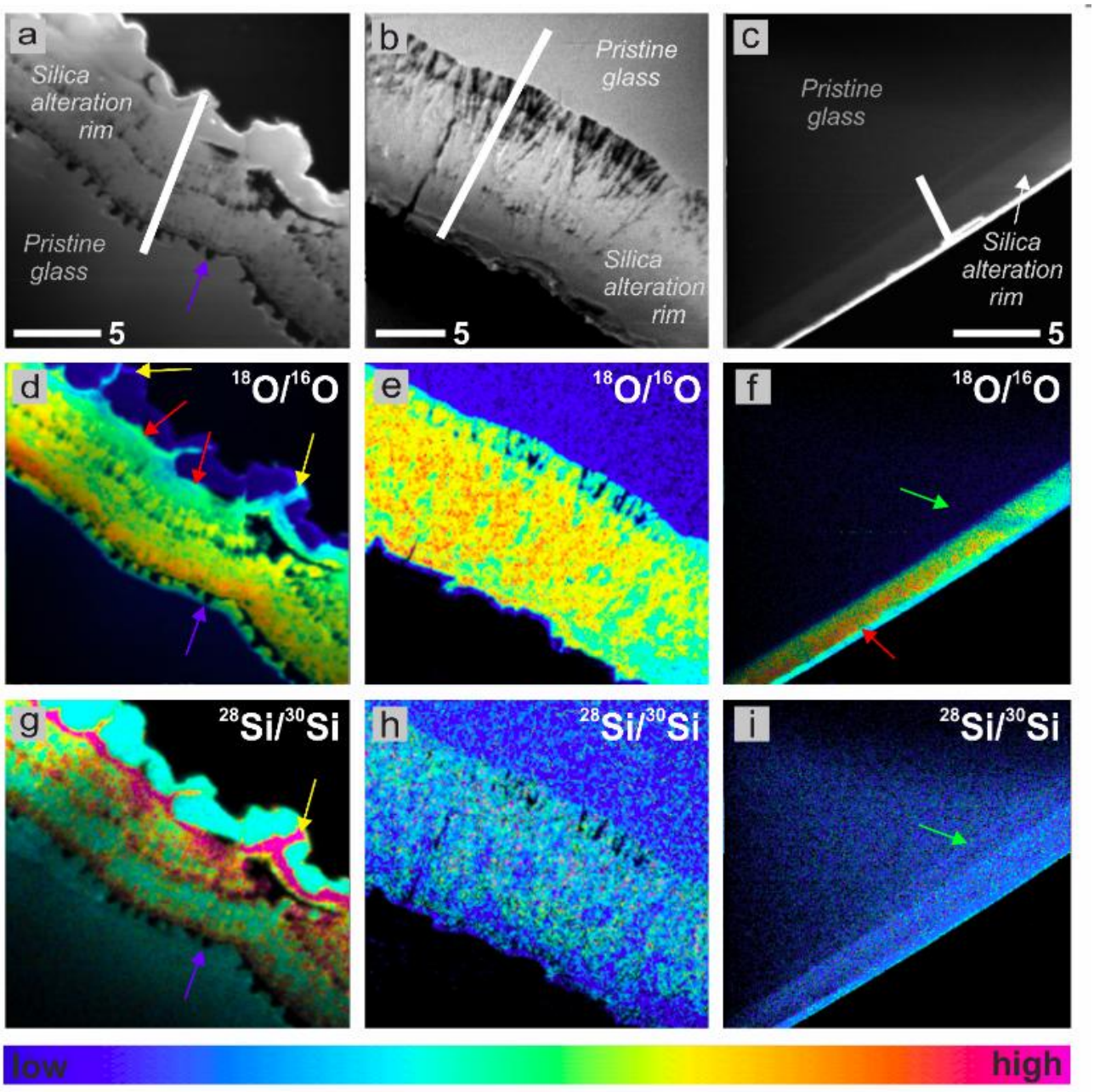

Fig. 10. Aqueous elemental release curves as a function of time measured during corrosion of SON68 glass. The non-stoichiometry of the normalized elemental release rates ($R_{Li} \approx R_B > R_{Cs} > R_{Si} \approx R_{Mo}$) was attributed to solubility control (*i.e.*, CIDR) within thin fluid film at pristine glass dissolution front. These data complement solid-state results for the 1-month sample shown in Figs. 7-8. Adapted from Fig. S4, Supp. Information, [27].